Computational Materials Science 192 (2021) 110319

Contents lists available at ScienceDirect

Computational Materials Science

journal homepage: www.elsevier.com/locate/commatsci

First-principles study of tensile and shear strength of an Fe_2Al_5//Fe interface

Muhammad Zeeshan Khalid [a,b,*], Jesper Friis [c,d], Per Harald Ninive [a], Knut Marthinsen [b], Inga Gudem Ringdalen [c], Are Strandlie [a]

[a] Department of Manufacturing and Civil Engineering, Norwegian University of Science and Technology, Gjøvik 2815, Norway
[b] Department of Materials Science and Engineering, Norwegian University of Science and Technology (NTNU), Norway
[c] SINTEF Materials and Chemistry, Trondheim, Norway
[d] Department of Physics, Norwegian University of Science and Technology, Trondheim, Norway

ARTICLE INFO

Keywords:
Fe-Al intermetallics
Tensile strength
Mechanical strength
Atomistic simulations
Face-to-face matching
Welding

ABSTRACT

The interfacial strengths of a low misfit Fe_2Al_5//Fe interface structure found at aluminum-steel joints has been studied using density functional theory. An interface between Fe and Fe_2Al_5 was selected based on a criteria of low lattice misfit and number of atoms. Through virtual tensile testing of bulk Fe_2Al_5 and the interface structures we show that the energy-displacement curve can be well described by including extra polynomial terms in the Universal Binding Energy Relation (UBER). It is shown that the Fe_2Al_5//Fe interface has a higher tensile strength than the bulk Fe_2Al_5 phase. We also find that the shear deformation process potentially can be initiated from an Fe-terminated interface.

1. Introduction

Owing to the increased interest in light-weight and environmental-friendly technology, Fe-Al compounds have been gaining increased industrial interest due to their light-weight, corrosion resistance and high-temperature resistance behavior [1–3]. However, the joining of aluminum and steel by traditional fusion welding techniques has been considered a main challenge due to the significant differences between their physical and chemical properties [4,5]. The intermetallic compounds (IMCs) which develop at the interface are normally not wanted, but unavoidable when welding aluminum and steel.

Various methods have been proposed and studied to join aluminum and steel [3,6]. For any method which requires high temperatures, a brittle layer of different types of Fe-Al IMCs is developed at the joint, making it difficult to obtain the desired joint strength. Although solid-state welding techniques can suppress the formation of Fe-Al IMCs at joints due to the low temperature, these methods can still not completely limit the formation of IMCs and can thus only produce Fe-Al joints with limited strength.

The thickness of the IMC layers also plays an important role in the strengthening of Fe-Al joints. It has been reported that the thickness of Fe-Al IMC layers formed in a brazed interface can be limited to less than 10 μm, which is considered as the critical thickness of a Fe-Al IMC layer for Fe-Al joints with good mechanical strength [7]. Analyses of Fe-Al joints suggest that the micro-structures and distribution of Fe-Al IMCs at the interface are dependent on heat input, and play an important role in determining the mechanical and/or corrosion behavior of the joints [8,9]. In general, most of the experimental and theoretical studies on Fe-Al IMC layers focus on, (i) heat input and thickness of the IMC layers [10] (ii) welding methodology [11,12] (iii) tensile and shear strength of IMC layers at the joint [3] and (iv) extended isothermal treatment [13–15].

Despite all these studies, the interfacial strength of intermetallics such as Fe_2Al_5//Fe has not been studied much in literature. Since it is thermodynamically possible to produce a range of Fe-Al compounds at the interface [16,17], it is necessary to understand the basic mechanical and interfacial strength of all these compounds to clarify their roles for the joint strength. The lack of convincing results for the interfacial strength is not due to a lack of academic and industrial interests on this important subject. However, due to the small thickness (2.3 ± 0.6 μm) of the IMC layers [18], it is very difficult to experimentally predict the interface strength of these compounds.

The above brief review indicates that the understanding of the behavior and strength of the individual interfaces of these compounds is

* Corresponding author at: Department of Manufacturing and Civil Engineering, Norwegian University of Science and Technology, Gjøvik 2815, Norway.
E-mail address: zeeshan.khalid039@gmail.com (M.Z. Khalid).

https://doi.org/10.1016/j.commatsci.2021.110319
Received 9 October 2020; Received in revised form 14 January 2021; Accepted 15 January 2021
Available online 18 February 2021

far from complete, and it is evident that an atomistic study of these interfaces could provide useful new insight. The lack of atomistic studies is due to the complex atomic structure of the intermetallic compounds. It is, therefore, challenging to develop an interface model which is periodic, simple and has a low lattice misfit. There have been many studies in literature for the determination of the interface structures between two bulk phases, e.g. [19–24]. Many different approaches such as O-lattice theory [25,26], the edge to edge model [27], the Conincidence of Reciprocal lattice point (CRLP) model [28] based on the Zur algorithm [22] have been developed to find and characterize the OR and conincidence of lattice between phases and grains. A major disadvantage of O-lattice theory is the lack of predictive capabilities, however the other approaches can successfully predict the OR, but they do not match the full structures. The edge to edge model considers the high density or nearly closed pack planes and direction and the CRLP and Zur algorithm match the underlying lattices of the structure ignoring the atoms inside them.

In this work, we have used a face-to-face matching technique to predict a possible Orientation Relationship (OR) between Fe_2Al_5 and Fe suitable for atomistic calculations.

This work is a follow-up of a project working on the role of IMC layers on the joining strength of aluminum and steel. Many distinct IMC layers have been observed at aluminium and steel joints, and computational calculations on several other Fe-Al IMC layers have already been published [29,30]. In order to make a consistent comparison between different Fe-Al IMC layers, the same assumption, methodology, and computational techniques were applied in this study and as in the other studies related to the Fe-Al IMCs [29,30].

The scope of this paper is limited to establish and test the modeling methodology for finding a good atomistic interface structure and to study the mechanical and interfacial properties of the relevant Fe_2Al_5// Fe interface. The structure of the paper is as follows. First, we present the procedure for finding a low misfit interface structure between Fe and Fe_2Al_5. In Section 3 we present the calculation methodology and procedure for performing virtual tensile calculations. In Section 4, we present results of the strength of the bulk Fe_2Al_5 as well as the Fe// Fe_2Al_5 interface structure. In the last section, we discuss the results before presenting a summary and conclusions.

2. Calculation methods and model

2.1. First-principles calculations

The first-principle calculations based on DFT were performed using the Vienna ab initio Simulation Package (VASP) [31]. The exchange–correlation energy was evaluated using the Generalized Gradient Approximation (GGA) by Perdew, Burke and Ernzerhof (PBE) [32] and with the Projector Augmented Wave (PAW) [33] method. By using the method proposed by Monkhorst–Pack to characterize energy integration as the first irreducible Brillouin zone [34] mesh size of $9 \times 5 \times 2$ for bulk Fe_2Al_5 and $9 \times 5 \times 1$ for Fe_2Al_5//Fe interface structures.Maximum energy cutoff value of 450 eV was used for the plane wave expansion in reciprocal space. During the optimization process, the change in total energy were converged to 10^{-5} eV. Furthermore, the average force per atom was reduced to 0.009 eV/Å using a smearing factor of 0.2 and first-order Meth-Paxton for the smearing of the partial occupation. Due to the magnetic behavior of Fe atoms, spin-polarized calculations were performed for the interface structures and bulk Fe by specifying the initial local magnetic moment of Fe.

2.2. Determination of bulk Fe_2Al_5

Fe_2Al_5 has an orthorhombic unit cell which contains single crystallographic Fe sites (four per cell) and three Al sites [35]. The Al1 site, which contains eight atoms per cell, is fully occupied, while Al2 and Al3 are too close to be occupied simultaneously, resulting in a partial occupancy factor of 1/6 for each of them [36]. We performed ground state energy calculations to find a stable crystal structure by calculating the formation enthalpy (ΔH_R) and cohesive energy (E_c) and used this structure further for bulk and interfacial calculations. The results of the bulk strength calculations of Fe_2Al_5 have been reported in a previous work [37] and can also be seen in Table 1.

Table 1
Calculated equilibrium lattice constants, cohesive energy (E_c) and formation energy (ΔH_R) for bulk Fe_2Al_5.

	Reference	a_0(Å)	b_0(Å)	c_0(Å)	E_c(eV/atom)	ΔH_R(eV/atom)
Fe_2Al_5	This work	7.418	6.428	4.103	−7.364	−7.352
	DFT[a]	7.466	6.181	4.808	−13.728	−8.352
	EAM[b]	7.622	6.323	4.178		
	Exp.[c]	7.675	6.403	4.203		

[a] [38]
[b] [39]
[c] [40]

2.3. Prediction of orientation relationships

In order to create a good representative periodic interface structure for the DFT calculations, a common supercell of two crystal surfaces forming an interface is required. However, in the general case the two crystals have different lattice constants, it is necessary to rotate the two crystals relative to each other in order to obtain an interface with as little strain as possible in order to get an as realistic as possible interface.it is challenging to find low strain interface structure without an excessive number of atoms in the supercell due to the huge number of possible orientation relationships and orientations of the habit plane. The benefit with our algorithm is that it actually finds, in a very efficient way, the optimal OR and habit plane orientation with minimum strain and a manageable number size of the supercell. Stradi et al. [21] developed an algorithm for the efficient and systematic search for common supercells between two crystalline surfaces. The method presented in this work is based on the same principles as presented by Stradi et al. First the equivalent directions of the two crystal surfaces are determined and rotated to match at the interface. Then, both crystals are equally strained to match at the interface. This results in different interface structures and ORs based on the number of atoms and low lattice misfit as presented in Table 6. This method provides an advantage of predicting a number of ORs between two crystals without an excessive number of atoms and low lattice misfit interface.

The first step in creating the interface structure is to establish an OR between the two phases in question. We modeled the interface as an atomically sharp defect-free interface between two crystals 1 (Fe) and 2 (Fe_2Al_5). To find possible ORs, a large number of possible sets of crystallographic directions were explored. The possible interface planes in Fe are defined by all pairs of lattice vectors, $\mathbf{u}_1$ and $\mathbf{v}_1$, in Fe. Similarly, $\mathbf{u}_2$ and $\mathbf{v}_2$ define all possible interface planes of Fe_2Al_5. To obtain a periodic interface, the following relations must be fulfilled:

$$\begin{aligned} |\mathbf{u_1}| &= |\mathbf{u_2}| \\ |\mathbf{v_1}| &= |\mathbf{v_2})| \\ \gamma_1 &= \gamma_2 \end{aligned} \tag{1}$$

where $\angle\,\gamma_n = \angle(\mathbf{u}_n, \mathbf{v}_n)$, with $n = 1, 2$ for crystal 1 and 2, respectively, and it is defined as the angle between vector directions $\mathbf{u}$ and $\mathbf{v}$. We have added a vacuum layer along the normal direction to avoid periodic interaction. For this reason, angles $\angle\,\alpha_n = \angle(\mathbf{v}_n, \mathbf{w}_n)$ and $\angle\,\beta_n = \angle(\mathbf{u}_n, \mathbf{w}_n)$ are not relevant, as the interface structures do not need to be periodic along the normal direction to the interface.

In the general case, it is not possible to find an OR satisfying these conditions exactly. The resulting interface structure depends on how well these conditions are fulfilled using the strains along direction $\mathbf{u}$ and

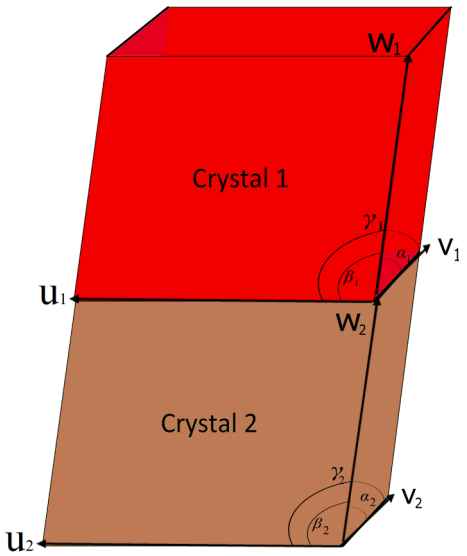

Fig. 1. A possible 3D interface model between crystal 1 and crystal 2. The crystals are slightly strained in order for them to match.

direction **v**:

$$\epsilon_u = \frac{||\mathbf{u}_2| - |\mathbf{u}_1||}{|\mathbf{u}_1| + |\mathbf{u}_2|} \tag{2}$$

$$\epsilon_v = \frac{||\mathbf{v}_2| - |\mathbf{v}_1||}{|\mathbf{v}_1| + |\mathbf{v}_2|} \tag{3}$$

and the difference in angles γ between the lattice directions;

$$\Delta\gamma = |\gamma_2 - \gamma_1| \tag{4}$$

These angles between two crystals are illustrated in Fig. 1. The two structures (red and brown) are strained to match the angles to form a coherent interface structure ($\gamma_{1,2} \neq 90^\circ$).

In general an interface structure has 9 degrees of freedom (3 degrees related to the possible OR, 2 degrees for the possible interface plane, 2 for lateral translation along the interface plane and 2 degrees for position of where the interface cuts each phase). Ideally, all $\Delta\gamma = 0$, but when these conditions are not fulfilled, the minimum difference between angles (min $\Delta\gamma$) can be considered.

To construct good interface models, ORs are obtained by looping through all possible combinations of orientations up to a given crystal lattice vector length and testing them against the criteria listed above. We can thereby choose an interface structure with a low misfit and a corresponding supercell structure with low enough number of atoms so that DFT calculations are feasible.

By using the methodology presented above, we have predicted the possible interface structures between Fe_2Al_5 and Fe. The DFT-relaxed bulk structure of Fe_2Al_5 was used as input for finding the interface structures. To reduce computational cost, we only considered interface structures where the number of atoms and misfit are relatively small (see Appendix Table 6). We considered different orientation relationships based on their compact planes and directions and calculated the work of separation. Since some of the interfaces are quite large, optimizing all structures with atomic relaxations is a computationally expensive and difficult task. However, to make reasonable comparisons and to find the best low energy interface OR, we built all interfaces using the same criteria, these criteria where that the interplanar spacing between two bulk phases at the interface were set to be 2.86 Å and the transverse layers were assured to have a thickness of 10 Å on each side of the phase. In addition a vacuum layer of 10 Å was added to avoid periodic interaction along the normal direction. In order to motivate the selection of a good representative interface, we calculated the work of separation for an assortment of low misfit ORs. The calculated values are shown in Table 2. We finally selected the interface structure that has a low misfit, the least number of atoms and and the largest value of the work of separation (3.58 J/m^2) for further investigations.

Table 2
Work of separation values for different ORs of Fe_2Al_5//Fe interface structures.

Interface	Work of separation (J/m^2)
Fe_2Al_5(0–20)//Fe(-121)	3.58
Fe_2Al_5(-1–20)//Fe(-343)	1.25
Fe_2Al_5(-200)//Fe(-343)	0.32
Fe_2Al_5(-200)//Fe(-323)	1.72
Fe_2Al_5(-110)//Fe(-121)	3.28
Fe_2Al_5(-120)//Fe(1–11)	2.40

2.4. $Fe_2Al_5(0\bar{2}0)//Fe(\bar{1}21)$ interface

The atomic structure of Fe_2Al_5//Fe was constructed using the procedure described above (Sec. 2.3). To ensure the bulk-like interior of atomic interfaces, six layers of Fe and Fe_2Al_5 were tested. It is worth mentioning that Fe_2Al_5 can be terminated either by Al or Fe at the interface. Both terminations were used for the interfaces shown in Fig. 2. To avoid periodic interactions, a vacuum layer of >10 Å was added along the normal direction to remove the effect of the two artificial interfaces. For the strength calculations, relaxed interface structures were used as an input for virtual tensile and shear test calculations.

2.5. Virtual tensile test calculations

Ab-initio virtual tensile calculations of the Fe_2Al_5//Fe interface were carried out in the framework of the Rigid Grain Shift (RGS) and RGS + relaxation methodology [41,42]. In this approach, the equilibrium structure was separated along the [0$\bar{2}$0] direction. For each displacement, two kinds of calculations were performed: (1) RGS, without any atomic relaxations, and (2) RGS followed by atomic relaxations with a fixed supercell. We did not consider Poisson's effect in this study [43]. The top two layers are fixed, while the remaining middle layers are allowed to relax during the RGS + relaxation procedure, and a vacuum is added at the interface to imitate the tensile tests, as illustrated in Fig. 3. The same procedure was applied for both bulk and interface structures.

In the RGS approach, the interface structure was modeled by rigidly separating the Fe slab along the normal **c** direction at the interface and performing static calculations without any electronic and atomic relaxations, while in the RGS + relaxation method, atoms were allowed to relax. The slabs were initially separated by gradually adding vacuum at the interface in steps of 0.2 Å. The tensile displacement step size was selected based on the following criteria: (i) try to sample fairly dense near zero displacement to get a good estimate for the second derivative, (ii) try to sample fairly dense near where we expect the inflection point to be (iii) have at least one point at high displacements for good determination of the binding energy. Due to the computational cost of the RGS + relaxation methodology, a non-uniform step size was selected at the higher separation distances to find the fracture zone of the interface structures. The fitting of calculated values with the analytical expression provides a reasonable approach for reducing computational cost by reducing the considered step sizes and it can also further be useful for providing qualitative comparative analyses with other Fe-Al IMC interfaces [29,30].

Rose et al. [44] observed that the separation energy of metals has a universal form;

$$E_b(d) = |E_b^e| \cdot g(a) \tag{5}$$

where E_b^e is the separation energy of the equilibrium structure, d is the displacement defined with respect to the equilibrium structure and a is the re-scaled displacement, given by $a = d/l$, where l is a characteristic

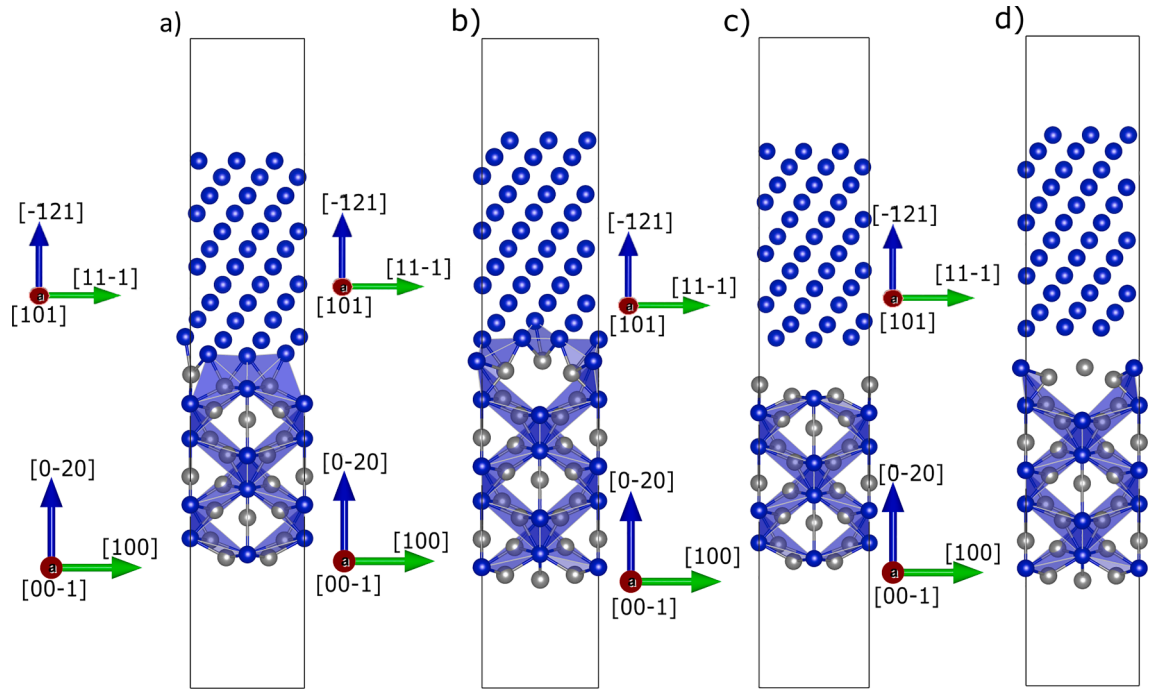

Fig. 2. Virtual tensile tests for the $Fe_2Al_5(020)$// Fe (-121) interface structure: (a, b) shows the Fe and Al-terminated relaxed equilibrium structures, (c) Fe-terminated virtual tensile test, and (d) Al-terminated virtual tensile test.

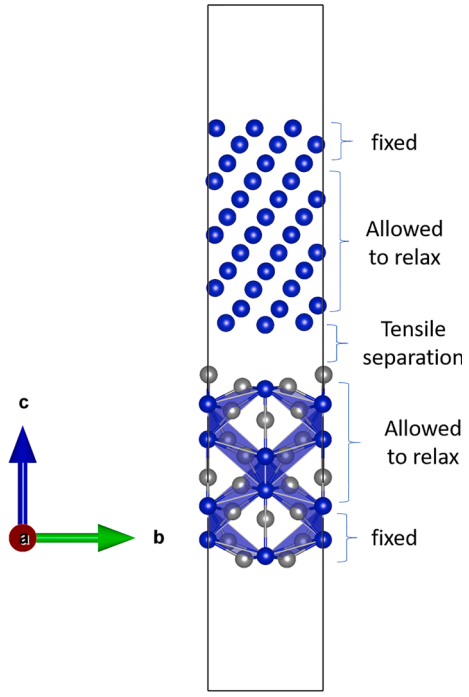

Fig. 3. Schematic illustration of the virtual tensile tests procedure.

length which can be approximated by the curvature of the energy-displacement curve at its minimum. Eq. (6) is used as a starting point for the fitting procedure,

$$l = \sqrt{\frac{|E_b^e|}{E_b''(0)}} \tag{6}$$

If the functional form $g(a)$ is known, we can determine the theoretical strength and critical displacement of any material from the parameters E_b^e, and E_b''. This virtual tensile testing provides separation energy versus tensile displacement. The results obtained from these calculations can then be fitted to the UBER curve using Eqs. (5) and (7) (below). As Rose et al. observed, the metallic bonding-energy curve can be approximately scaled into the universal binding energy relation for the following cases: (i) metallic or bimetallic adhesion (ii) chemisorption on a metal surface, and (iii) cohesion of bulk metals [44]. Although UBER describes well separation energy versus displacement for unrelaxed metal surfaces, it is unable to describe the behavior of tightly bound intermetallics [45]. To find a good fit which captures the behavior of the separation energy versus displacement curve, we used a generalized form which includes two polynomials [46,30]:

For the hydro-static compression/expansion, $g(a)$ was determined to be [46]:

$$g(a) = -(1 + a + P(a))e^{-a-Q(a)} \tag{7}$$

where a is the rescaled displacement and P and Q are polynomials of order two or larger with positive (leading) coefficients. This expression for $g(a)$ ensures that $g(0) = -1, g(a \to \infty) = 0$ and $g'(0) = 0$. The first-order terms are excluded from P and Q since they are related to each other as well as to the characteristic length.

To ensure that the fitting behaves well, one should only include odd-order terms in the polynomials P and Q and make sure that all coefficients are zero or positive.

By differentiating the fitted energy-displacement curve, the theoretical tensile strength of the atomic structures can be evaluated [47];

$$\sigma_{th} = \frac{\partial E_b}{\partial d} \tag{8}$$

The theoretical strength σ_{th} at its maximum value is defined as the Ultimate Tensile Strength (σ_{UTS}). The value of d at σ_{UTS} is defined as the critical length d_c.

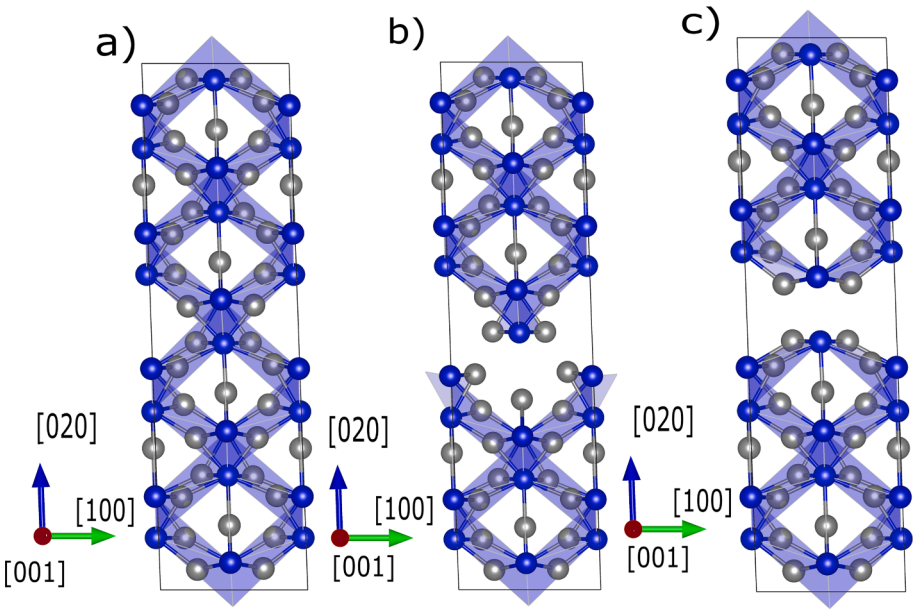

Fig. 4. Virtual tensile tests for the bulk Fe_2Al_5(020) structure: (a) relaxed equilibrium structure (b) Al-terminated virtual tensile test, and (c) Fe-terminated virtual tensile test.

3. Results and discussion

3.1. Bulk strength

To compare the bulk and interface structures, we also calculated the tensile properties of $Fe_2Al_5(0\bar{2}0)$ using the rigid shift (RGS) and RGS + relaxation methodology as explained in Sec. 3.1. We studied the virtual tensile strength of both the Al- and the Fe-terminated Fe_2Al_5 structures as shown in Fig. 4.

Fig. 5 (a) and (b) show the separation energy versus tensile displacement curve for Al and Fe-terminated fractures using the RGS and RGS + relaxation methodologies, respectively. In the stable configuration of the Fe_2Al_5 phase, the Fe-Al bond distance is 2.50 Å and the Fe-Fe bond distance is 2.96 Å. During the virtual tensile testing, this bond distance at the cutting plane is stretched further until the bulk structure fractures and separates into two free surfaces. Fig. 4 (b) and (c) show the procedure for introducing a crack with Al and Fe-terminations. Table 3 lists the work of separation (W_{sep}) and the work of adhesion (W_{ad}). The former is defined as the work needed to separate a bulk phase without atomic relaxations, and the latter is the energy needed to separate a bulk interface into two relaxed surfaces [48].

The binding energy increases with tensile displacement. RGS without atomic relaxation produces a steeper curve which was fitted using Eqs. (5) and (7). During tensile displacement, the separation energy increases sharply until it stabilizes at larger displacements (> ~5 Å).

Table 3 lists the calculated values of σ_{UTS}. Fig. 6 shows the stress–strain curves for Fe_2Al_5 along with bulk strengths for the RGS and RGS + relaxation methodologies. With increasing tensile strain, the tensile stress increases until its maximum value (σ_{UTS}). One can note that σ_{UTS} calculated with the RGS + relaxation methodology is lower than that for the RGS methodology. For comparisons, we also present the strength of the bulk Fe (111) plane. The Al-terminated Fe_2Al_5 bulk phase shows higher strength (20.09 GPa for RGS and 15.48 GPa for RGS + relaxation) as compared to the Fe-terminated structure (17.72 GPa for RGS and 13.28 GPa for RGS + relaxation). Moreover, the bulk Fe structure shows higher values of W_{sep} and σ_{UTS}, which signify the higher strength of bulk Fe than that of the Fe_2Al_5 phase. A lower strength of the Fe-terminated bulk Fe_2Al_5 structure indicates a weaker bonding between Fe-Fe atoms which will be discussed in sub-Section 4.3. Besides, the long bonding distance between Fe-Fe also contributes to the weakening of the bond.

3.2. Interface strength

3.2.1. Energy-displacement curves

Energy-displacement curves are shown in Fig. 7 for Al-terminated and Fe-terminated interface structures using the above-mentioned fitting technique. Fig. 7 (a) and (c) show the energy-displacement curve for RGS and Fig. 7 (b) and (d) show the same curves for the RGS + relaxation methodology. A steep and continuous curve is obtained for the RGS methodology without any atomic relaxations, which can be fitted well by using Eq. (5). As can be seen from Fig. 7(b) and (d), with increasing in tensile displacement, the energy required to fracture the interface structure decreases until the structure separates into two surfaces at larger displacements (>3 Å). The separation length at this point is defined as the final fracture length (d_f). Even though there is no unique way of determining d_f, we here define it to be at the point where the binding energy curve reaches −0.003 eV/Å^2 [30].

The minimum value of the binding energy gives $-E_b(0) = W_{sep}$ for RGS and $-E_b(0) = W_{ad}$ for the RGS + relaxation methodology. Table 4 lists the W_{sep} and W_{ad} values for the Fe_2Al_5//Fe interface. As given in Table 4, the Al-terminated interface shows higher W_{sep} (4.45 J/m^2) as compared to the Fe-terminated interface (3.82 J/m^2). Lazar [41] postulated the rough approximation that W_{sep}= 1.06 W_{ad} by linear fitting of DFT results of RGS and RGS + relaxation methodologies for different compounds and materials. This fits perfectly for the Al-terminated interface but less so for the Fe-terminated interface.

An optimal fit for the relaxed surfaces is shown in Fig. 7 (b) and (d). For the relaxed-type virtual tensile tests, crack opening is initiated by separating two blocks by introducing vacuum and subsequently allowing atoms to relax while keeping the plane area fixed. The initial crack introduced during RGS can potentially be healed by atomic relaxations if the separation between the two blocks is smaller than the critical length (d_c) [47]. In Fig. 7 (b) and (d), d_c is located at the border of Region I ($d < d_c$). Table 4 lists the critical (d_c) and fracture lengths (d_f) for the two relevant interface structures.

Region II is defined for separations $d_c < d < d_f$. In this region, the structure is neither separated nor being able to heal by elastic relaxations, which is why it is defined as the instability region. The range of this instability region is determined by taking the difference between d_f and d_c. The width of Region II is related to the brittleness/ductility of the interface structure [41]. For the Al-terminated interface structure,

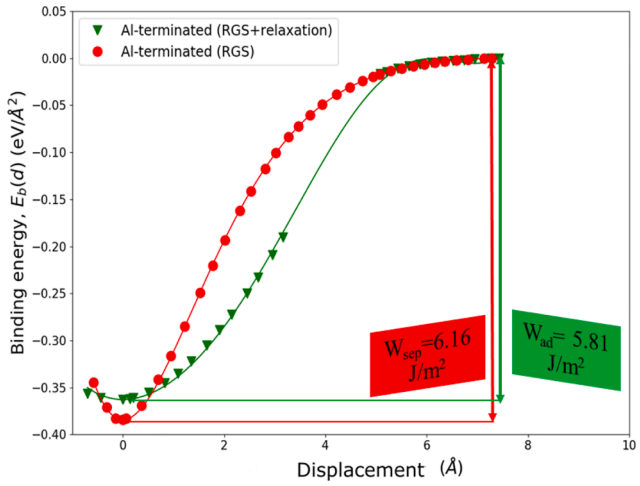

(a) Al-terminated bulk Fe_2Al_5.

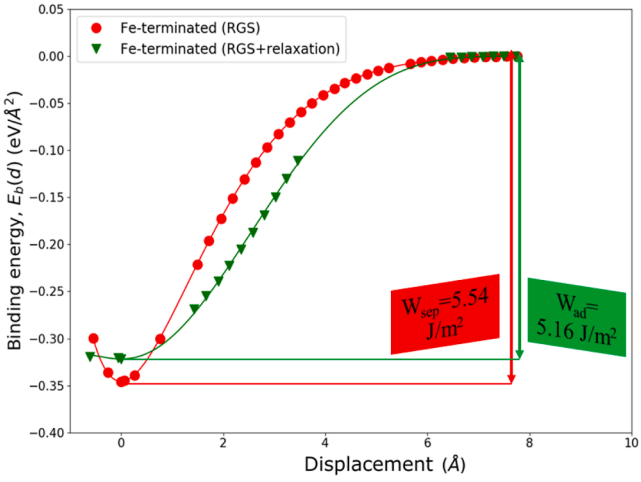

(b) Fe-terminated bulk Fe_2Al_5.

Fig. 5. Separation energy versus displacement for virtual tensile tests of the bulk Fe_2Al_5(020) structure: (a) Al-terminated virtual tensile test, and (b) Fe-terminated virtual tensile test.

Table 3
Calculated ultimate tensile strength, W_{sep} and W_{ad} of bulk Fe_2Al_5 and bcc Fe.

Structure	σ_{UTS} (RGS) (GPa)	σ_{UTS} (RGS + relaxation) (GPa)	W_{sep} (J/m^2)	W_{ad} (J/m^2)
Al-terminated Fe_2Al_5	20.09	15.48	6.16	5.81
Fe-terminated Fe_2Al_5	17.72	13.28	5.54	5.16
Fe	27.7[a] < 111 > 28.5[b,c] < 111 >	–	6.09 < 121 >	–

[a] [49]
[b] [50]
[c] [51]

the length of the instability region is approximated to be 0.84 Å, while for the Fe-terminated interface, it is 0.79 Å. The shorter range of the instability region for the Fe-terminated interface indicates a more brittle fracture than that of the Al-terminated interface.

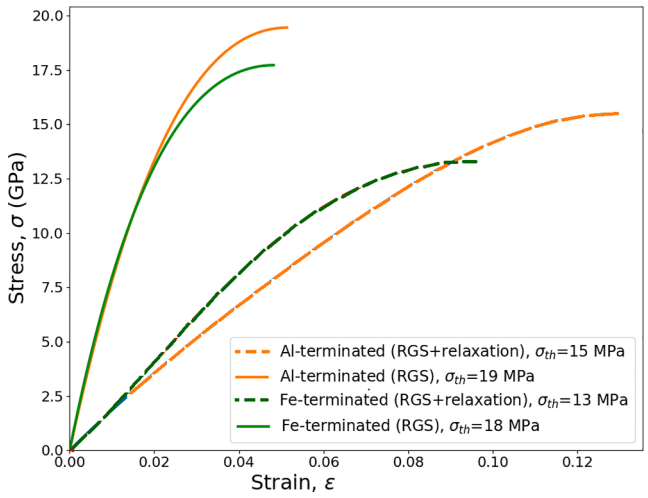

Fig. 6. Virtual tensile tests stress–strain curve for the bulk Fe_2Al_5(020) structure with both Al and Fe-terminations calculated with the RGS and RGS + relaxation methods.

At longer separation distances ($d > d_f$), the interface structures are completely separated into two relaxed bulk surfaces. This region is defined as Region III in light grey color (Fig. 7 (b) and (d)). In this region, there is no interaction at the interface, and relaxation of the atomic positions relaxes the bulk surfaces into stable configurations. For this reason, the binding energy versus separation curve stabilizes, and no further increase in binding energy can be seen.

3.2.2. Tensile strength

Table 4 lists σ_{UTS} of Fe_2Al_5// Fe interface structures for both terminations. Since RGS + relaxation calculations were performed with atomic relaxations, σ_{UTS} calculated from this approach provides more realistic values than those for the RGS calculations. Based on the RGS + relaxations virtual tensile tests, the Al-terminated interface shows lower strength (23.88 GPa) as compared to the Fe-terminated interface (31.48 GPa). Overall, the interface structures show higher σ_{UTS} values than bulk Fe_2Al_5. The Fe-terminated interface shows the highest strength (31.48 GPa) and Fe-terminated bulk Fe_2Al_5 the lowest strength (17.72 GPa).

In order to elucidate the bonding characteristics of the interfacial and bulk atoms, total charge density isosurfaces and charge density difference plots for all surfaces were constructed as shown in Fig. 8. A high charge density cloud (labeled as B in Fig. 8(c)) can be seen for the Fe-terminated interface as compared to the Al-terminated interface (labeled as A in Fig. 8(a)). Moreover, there is a higher charge transfer for the Fe-terminated interface, while there is a weak charge transfer zone for the Al-terminated interface as shown in yellow color in Fig. 8(b). This high charge density and transfer rate at B indicates stronger bonding between interfacial Fe-Fe atoms at the Fe-terminated interface, which explains the higher σ_{UTS} for this interface as compared to the Al-terminated interface.

For the bulk Fe_2Al_5 structure as shown in Fig. 8(e-f), Fe-Fe bonding (labeled as C) was found to be weaker than the Al-Fe bonding (labeled as D). This observation is consistent with the lower σ_{UTS} for the Fe-terminated bulk structure. Generally, Fe-Al atoms are found to have higher charge density and charge transfer regions at the interfaces and in the bulk structures. However, in the Al-terminated interface, the Al atoms move towards the Fe atoms and develops a bond at the interface by compromising the bonding strength at the first layer of the Fe_2Al_5 side, labeled as I in Fig. 8(a). This fracture plane can be a weak link of the overall Al-terminated interface structure.

3.2.3. Ideal shear strength

To calculate the ideal shear strength a series of incremental shear

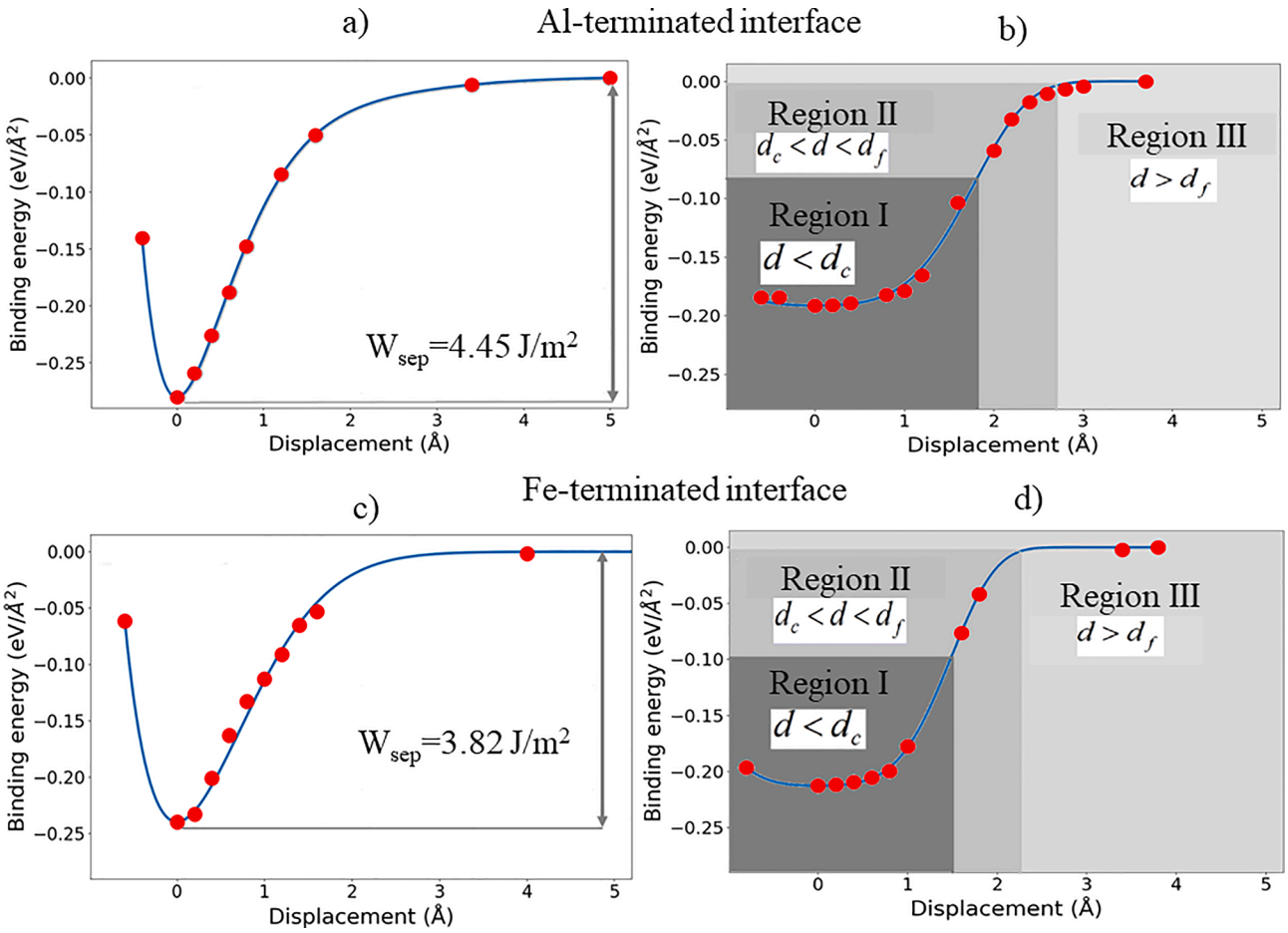

Fig. 7. Energy-displacement curves resulting from virtual tensile tests for the Fe_2Al_5(020)//Fe interface structure with both Al and Fe terminations, (a) and (c) show the virtual tensile test results for the RGS methodology and (b) and (d) for the RGS + relaxation methodology. Red points show DFT calculation results and the blue solid line is the fitted curve.

Table 4
Calculated ultimate tensile strengths, W_{sep} and W_{ad} values of the Fe//Fe_2Al_5 interface structure.

Structure	σ_{UTS} (RGS) (GPa)	d_c (Å)	d_f (Å)	σ_{UTS} (RGS + relaxation) (GPa)	W_{sep} (J/m^2)	W_{ad} (J/m^2)
Al-terminated interface	29.56	1.80	2.64	23.88	4.45	3.04
Fe-terminated interface	24.50	1.51	2.30	31.48	3.82	3.36

strains were applied to the Fe_2Al_5//Fe supercell. We moved the Fe surface along the $< 001 >$ and $< 001 >$ shear directions. For these calculations, six layers of Fe were sheared along the defined shear directions with respect to the Fe_2Al_5 atoms at the interface. Atoms were allowed to relax along the normal direction to the interface to remove any strain along that direction. The shear energies are defined in terms of a Fourier series;

$$E_s(d) = E_0 + \sum_{n=1}^{\infty}[A_n cos(k_n d) + B_n sin(k_n d)] \quad (9)$$

where $E_s(d)$ and E_0 are the energy of the displaced and unsheared structure, respectively, d is the shear displacement, and $k_n = \frac{2\pi n}{\lambda}$, where λ is the periodicity along the shear direction. Appendix Table 5 and 6 gives the Fourier series coefficient values and the value of λ for both interface structures.

The shear stress is given by

$$\gamma_s = \frac{1}{A}\frac{\partial E_s}{\partial d} \quad (10)$$

where A is the interface area. The maximum value in the resulting shear-displacement curve corresponds to the ideal shear strength, which is defined as the interface resistance to the shear displacement after which it starts to deform.

Fig. 9 shows the stress-displacement curve for the shear stress as a function of shear displacement for both Al- and Fe-terminations. Initially, stress increases with the increase in the shear displacement until it reaches a maximum value for both cases, which is taken as the ideal shear strength of the interface structure. Table 5 summarizes the ideal shear strength of the Fe_2Al_5//Fe interface structure for the different cases discussed in this work. Results are quite different for both interface terminations. The Fe-terminated interface shows low shear strength (0.97 GPa) along $< 001 >$ and larger shear strength along $< 100 >$ (4.74 GPa), while the Al-terminated interface shows high shear strength (2.51 GPa) along the $< 100 >$ direction and a slightly lower shear strength along $< 001 >$ (3.97 GPa). In general the Al-terminated structure shows higher shear strength than the Fe-terminated interface structure. These calculations, therefore, indicate that the Fe-terminated $< 001 >$ interface is more prone to shear failure than the Al-terminated interface.

Comparing shear strength with tensile strength indicates that the Al-terminated interface shows higher tensile and shear strength than the Fe-terminated interface. From Table 4 and 5, it can be seen that shear

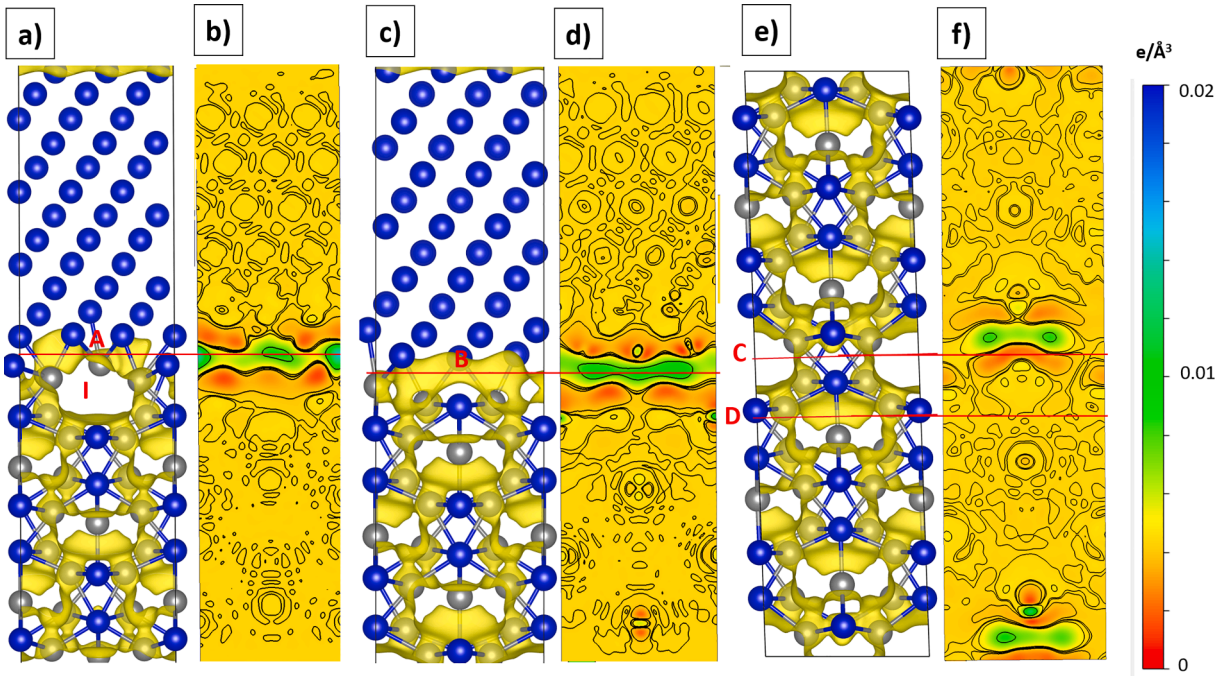

Fig. 8. Calculated total charge density isosurfaces (a,c,e) drawn at 0.03 e/Å^3 and charge density difference plots (b,d,f) for (a-b) Al-terminated interface, (c-d) Fe-terminated interface and (e-f) bulk Fe_2Al_5. A, B, C, and D define the cutting planes for virtual tensile testing and I indicates the weak fracture plane for the Al-terminated interface.

Table 5
Calculated Ideal shear strength values of the Fe_2Al_5 $(0\bar{2}0)$//Fe$(\bar{1}21)$ interface, directions are defined with respect to Fe_2Al_5.

Interface	<001> (GPa)	<100> (GPa)
Fe-termination	0.97	4.74
Al-termination	3.97	2.51

instability can occur earlier than normal decohesion. This is consistent with the experimental observations of an Al-Fe welded system [52]. The shear strength calculated in this study for loading parallel to the interface is lower than the perpendicular loading direction (σ_{UTS}). The same trend has been observed experimentally and theoretically in the literature [16,52,53].

4. Discussion

Before discussing the implications of these results, some limitations are worth to be mentioned. These simulations have been performed without considering dislocations, micro-voids, and other effects occurring at larger length scales, that will obviously influence the strength of real joints [54]. Hence, the calculated strengths are thus generally overestimated. Still, these calculations provide important insights about the crack formation mechanism of the interface structure at the atomic

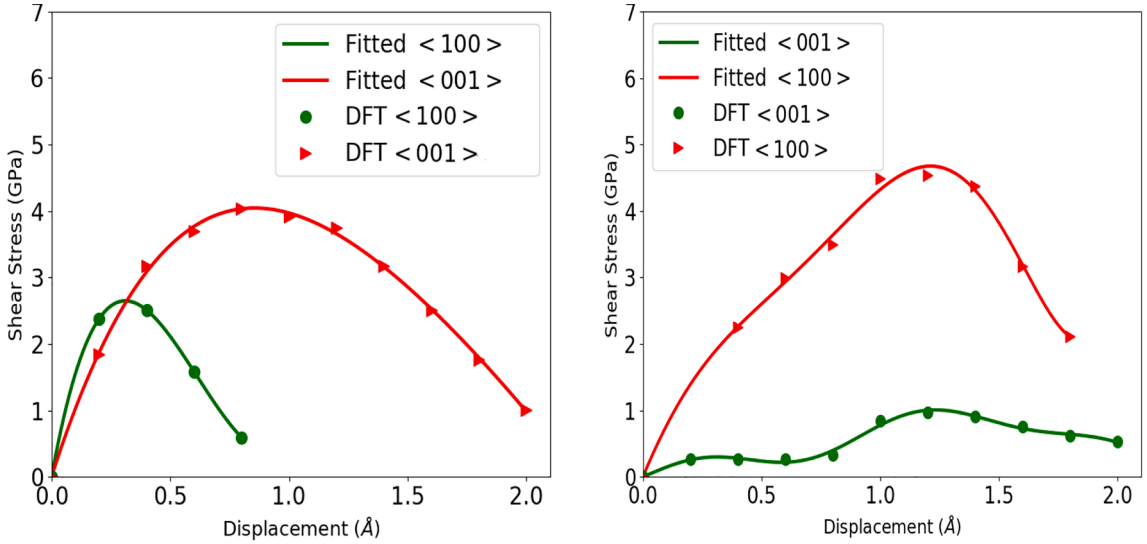

Fig. 9. Fitted shear stress-displacement curve of the Fe_2Al_5//Fe interface for (a) Al- and (b) Fe-terminations during the shear strength calculations as a function of shear displacement along the < 001 > and < 100 > shear directions.

scale. The role of crystal defects on the mechanical properties is proposed to be a subject of future studies.

In this work we have studied the effect the Fe_2Al_5 intermetallic phases has on the strength of an aluminium-steel joints. It is a very difficult task to identify the fractured layer of aluminum and steel joints by experiments. For this reason, to predict the weak zone of the Fe_2Al_5// Fe interface structure, two zones were studied: (i) bulk Fe_2Al_5 and (ii) Fe_2Al_5//Fe interface. Based on bulk and interface calculations, the interface between Fe_2Al_5// Fe showed higher strength as compared to bulk Fe_2Al_5 and smaller than bulk Fe [49]. Virtual tensile testing, therefore, indicates that bulk Fe_2Al_5 is more prone to induce fracture than the interface and bulk Fe side. Mechanical strength inferred from the virtual tensile calculations indicates that fracture is most likely to be initiated from the Fe-terminated side of the bulk Fe_2Al_5 due to weak bonding between Fe-Fe atoms. Shear strength is seen to be lower than the tensile strength, which is also consistent with the experimental observation of Fe_2Al_5 [55].

We have performed more calculations with the strained interface structures to study the effects of elastic strain on work of separation. All calculations were performed considering the optimized equilibrium interface structures. As discussed in Section 2, both bulk slabs were strained to match at the interface. In order to determine the elastic contribution to the work of separation, calculations were performed to determine the work of separation for the strained interface structures and the results are compared with those of the equilibrium interface structure. In the case of the Fe-terminated interface, the work of separation was reduced from 5.54 J/m^2 to 3.58 J/m^2. However, for the Al-terminated interface the work of separation was drastically reduced: from 6.16 J/m^2 to 2.91 J/m^2. This indicates that the failure mechanism for the interface structure might be more complex than what can be described using this method and should be investigated in more detail in further work.

Moreover, the theoretical tensile strengths of an interface structure depends on the number of crystallographic layers of the model. A recent study [56] has indicated the decrease in fracture stress with increasing supercell size with localized strain models. Effect of supercell size is beyond the scope of this study. Moreover, as the main objective is to make a comparative analysis of Fe-Al IMCs interfaces, we adopted a consistent methodology and approach for all interface structures to make appropriate qualitative comparisons. However, further investigations are needed to find the influence of the number of layers on the strength values for the RGS + relaxation methodology. Since this study is limited to the DFT methodology, it presents an extra challenge of computational cost. This is why the values obtained from the RGS + relaxation method only provides qualitative comparative strength of the Fe//IMC interface as compared to the Al/IMC [29], IMC//Fe and pure IMC//IMC interfaces [30]. Still we believe this provides useful insights into the role of Fe-Al IMCs on the joining of aluminium and steel.

In general, these results have a particular significance for the welding of aluminum and steel joints for different welding methodologies, where the presence of an Fe_2Al_5 intermetallic layer has been reported along the steel side. However, the defects at the IMC layers also play a significant role in deteriorating the joint strength and have to be included in the calculations to give more reliable predictions for real systems in the future.

5. Summary and conclusions

To summarize, we have performed DFT calculations of tensile and shear strength of the Fe_2Al_5//Fe interface. The interface structure with the lowest lattice misfit and number of atoms was selected for the DFT calculations of this work. Virtual tensile tests were performed with the rigid grain shift (RGS) methodology without atomic relaxations and RGS + relaxation methodology with atomic relaxations. Polynomial terms were introduced into the UBER to find a reasonable fit for the tensile stresses. Based on RGS calculations, the Al-terminated interface showed higher strength than bulk Fe_2Al_5 and the Fe-terminated interface structure. During the relaxation of atomic positions in the RGS + relaxation methodology, the tensile strength decreased for all structures except for the Fe-terminated interface. Moreover, the charge density maps indicated a weaker bonding between Fe-Fe atoms in the bulk Fe_2Al_5 structure, which contributed to a lower tensile strength. We also analyzed the shear strength for the interface along $< 001 >$ and $< 100 >$ directions. We found that $< 001 >$ has lower shear strength for the Fe-terminated interface while it showed higher strength for the Al-terminated interface.

Overall the Fe bulk side was found to be the strongest zone of the Fe_2Al_5//Fe interface structure followed by the interface and bulk Fe_2Al_5. Based on these calculations, it can be anticipated that during a mechanical failure, fracture is most likely to be initiated at the bulk Fe_2Al_5 side. This study can potentially be the starting point for further investigations of the effects of crystal defects and temperature on the joint strength of aluminum-steel joints.

CRediT authorship contribution statement

Muhammad Zeeshan Khalid: Conceptualization, Software, Data curation, Visualization, Investigation, Validation, Formal analysis, Writing - original draft, Writing - review & editing. **Jesper Friis:** Methodology, Software, Data curation, Formal analysis, Supervision, Writing - review & editing, Conceptualization, Validation. **Per Harald Ninive:** Methodology, Software, Supervision, Resources, Writing - review & editing. **Knut Marthinsen:** Supervision, Project administration, Writing - review & editing. **Inga Gudem Ringdalen:** Methodology, Writing - review & editing. **Are Strandlie:** Conceptualization, Methodology, Supervision, Project administration, Resources, Writing - review & editing, Funding acquisition.

Declaration of Competing Interest

The authors declare that they have no known competing financial interests or personal relationships that could have appeared to influence the work reported in this paper.

Acknowledgements

The work reported in this paper was based on activities within the centre for research-based innovation SFI Manufacturing in Norway and is partially funded by the Research Council of Norway under contract number 237900. UNINETT Sigma2 AS (The Norwegian Metacenter for High Performance Computing) provided computational resources through Project NN9466K and NN9158K.

Appendix A

Appendix Table 6 lists the predicted ORs between Fe and Fe_2Al_5 by the face-to-face matching technique. In Table 6, m_1, m_2 and m_3 are the components of a linear combination of vector $\mathbf{u_1}$ of crystal 1, similarly n_1, n_2 and n_3 are defined for crystal 2, and is given as;

$$\begin{aligned}\mathbf{u_1} &= m_1\mathbf{a_1} + m_2\mathbf{b_1} + m_3\mathbf{c_1}\\ \mathbf{u_2} &= n_1\mathbf{a_2} + n_2\mathbf{b_2} + n_3\mathbf{c_2}\end{aligned} \tag{11}$$

Table 6
Some of the predicted ORs between Fe_2Al_5 and Fe atoms. m_1, m_2 and m_3 are the direction vectors for Fe_2Al_5 phase and n_1, n_2 and n_3 for Fe atoms. length and strain (%) are the length of supercell and misfit percentage (as defined in Eq. (2) and (3)) of the interface structures respectively.

#	d	m_1	m_2	m_3	length (Å)	$\angle\gamma$	n_1	n_2	n_3	length (Å)	$\angle\gamma$	strain (%)	# atoms
1	u	0	0	−1			1	0	1			0.89	
	v	1	0	0	4.10	90°	1.5	1.5	−1.5	4.06	90°	0.79	64
	w	0	−2	0	7.40	90°	−2	4	2	7.46	90°		
	h	0	−2	0	12.88	90°	−1	2	1	14.06	90°	0.56	
2	u	0	0	0			1	0	1			0.89	
	v	2	0	0	4.10	119.9°	3.5	1.5	−3.5	4.06	119.8°	0.39	130
	w	−1	−2	0	14.80	90°	−3	4	3	14.84	90°		
	h	0	−1	0	14.86	90°	−3	14	3	16.73	90°	0.52	
3	u	0	0	1			1	0	1			0.89	
	v	1	2	0	4.10	119.9°	3.5	1.5	−3.5	4.06	119.8°	0.90	130
	w	−2	0	0	14.86	90°	−3	4	3	14.84	90°		
	h	−2	1	0	14.80	90°	−3	14	3	16.73	90°	0.56	
4	u	0	0	1			1	0	1			0.89	
	v	1	2	0	4.10	119.9°	3	3	−3	4.06	119.5°	0.38	116
	w	−2	0	0	14.86	90°	−3	2	3	14.91	90°		
	h	−2	1	0	14.80	90°	−1	2	1	13.46	90°	0.63	
5	u	0	0	1			1	0	1			0.89	
	v	0.5	1.5	0	4.10	101.1°	0.5	3.5	−0.5	4.06	101.4°	0.96	98
	w	−2.5	0.5	0	10.35	90°	−3	0	3	10.25	90°		
	h	−3	1	0	18.77	90°	−7	2	7	12.18	90°	0.71	
6	u	0	0	1			1	0	1			0.89	
	v	0.5	1.5	0	4.10	101.1°	2.5	0.5	−2.5	4.06	101.4°	0.96	98
	w	−2.5	0.5	0	10.35	90°	−1	4	1	10.25	90°		
	h	−3	1	0	18.77	90°	−1	10	1	12.18	90°	0.71	
7	u	0	0	1			1	0	1			0.89	
	v	1	2	0	4.10	110°	1	5.0	−1	4.06	110.3°	0.38	165
	w	−2.5	0.5	0	14.86	90°	−4.5	−0.5	4.5	14.91	90°		
	h	−2	1	0	18.77	90°	−5	2	5	18.32	90°	0.60	
8	u	0	0	1			1	0	1			0.89	
	v	0.5	0.5	0	4.10	97.9°	1	1	−1	4.06	98.0°	1.35	41
	w	−1.5	1.5	0	4.90	90°	−2	3	2	4.97	90°		
	h	−1	1	0	14.71	90°	−1	2	1	11.83	90°	0.80	
9	u	0	0	1			1	0	−1			0.89	
	v	1	0	−1	4.10	115.8°	−1.5	2.5	0.5	4.06	115.2°	0.40	56
	w	−1	2	0	8.46	90°	3	−1	3	8.49	90°		
	h	0	1	0	14.86	119.0°	5	2	5	12.51	118.6°	0.87	
10	u	0	0	1			1	0	−1			0.89	
	v	1.5	−0.5	−1	4.10	105.2°	−1	4	−1	4.06	105.9°	0.67	98
	w	0	2	0	12.26	90°	−3.5	−1.5	3.5	12.18	90°		
	h	1	3	0	12.88	109.5°	−1	0	1	14.84	109.5°	0.84	
11	u	0	1	2			3	0	−2				
	v	1	−1	1	10.42	119.2°	1	−3	2	10.35	119.6°	0.68	192
	w	0.5	1.5	−2	10.63	92°	−2.5	−0.5	−3.5	10.74	91.8°	11	
	h	3	2	−1	13.20	94.1°	−6	−8	−9	12.43	94.3°		
12	u	1	0	0			2.5	0.5	0.5			0.79	
	v	−0.5	1.5	2	7.40	95.8°	−0.5	0.5	−4.5	7.46	95.9°	0.92	215
	w	0	−2	3	13.19	90°	−1	4	1	137	90°		
	h	0	−4	3	17.81	106.3°	−5	22	3	12.18	105.9°	0.69	
13	u	0	1	−2			3	2	0			0.71	
	v	0.5	−1.5	1	10.42	109.4°	−1.5	0	−3.5	10.35	109.5°	0.94	230
	w	−2	0	0	11.13	90°	−2	3	3	112	90°		
	h	−8	−2	−1	19.38	104.3°	−14	21	9	13.46	104.6°	0.65	

Table 7
The fitting Fourier series coefficient values for the shear strength calculation of Al-terminated Fe_2Al_5//Fe interface.

Polynomial terms	A_0	A_1	A_2	A_3	B_1	B_2	B_3	λ
< 100 >	−1107.76	110.59	1864.90	−646.56	271.21	11115	−803.98	77.85
< 001 >	−1107.76	110.59	1864.90	−646.56	271.21	11115	−803.98	77.85

Table 8
The fitting Fourier series coefficient values for the shear strength calculation of Fe-terminated Fe_2Al_5//Fe interface.

Polynomial terms	A_0	A_1	A_2	A_3	A_4	A_5	B_1	B_2	B_3	B_4	B_5	λ
< 100 >	1660.13	−988.84	−3113.83	−1627.44	1624.54	−357.08	−299.39	1794.44	−4305.2	3842.35	−1144.45	106.08
< 001 >	0.415	−0.469	0.058	−0.0014	-	-	0.052	0.0699	0.0153	-	-	8.23

Normally m_1, m_2, m_3 and n_1, n_2, n_3 are integers, but due to sub-lattice translations in the conventional cell, fractions are also possible. Tables 7 and 8 lists the Fourier series coefficient values for the shear strength calculations for both interface structures.

References

[1] A. Hotař, M. Palm, P. Kratochvíl, V. Vodičková, S. Daniš, High-temperature oxidation behaviour of Zr alloyed Fe_3Al-type iron aluminide, Corros. Sci. 63 (2012) 71–81.

[2] B.L. Silva, A. Garcia, J.E. Spinelli, The effects of microstructure and intermetallic phases of directionally solidified Al-Fe alloys on microhardness, Mater. Lett. 89 (2012) 291–295.

[3] T. Sakiyama, G. Murayama, Y. Naito, K. Saita, Y. M. H. Oikawa, T. Nose, Dissimilar metal joining technologies for steel sheet and aluminum alloy sheet in auto body, Nippon Steel & Sumitomo Metal Corp., Tokyo, Nippon Steel Technical Report 103 (2013) 91–98.

[4] T. Ogura, Y. Saito, T. Nishida, H. Nishida, T. Yoshida, N. Omichi, M. Fujimoto, A. Hirose, Partitioning evaluation of mechanical properties and the interfacial microstructure in a friction stir welded aluminum alloy/stainless steel lap joint, Scripta Mater. 66 (8) (2012) 531–534.

[5] H. Das, S. Basak, G. Das, T.K. Pal, Influence of energy induced from processing parameters on the mechanical properties of friction stir welded lap joint of aluminum to coated steel sheet, Int. J. Adv. Manuf. Technol. (2013) 1–9.

[6] S. Imaizumi, Welding of aluminium to dissimilar metals, Welding Int. 10 (8) (1996) 593–604.

[7] S. Yang, J. Zhang, J. Lian, Y. Lei, Welding of aluminum alloy to zinc coated steel by cold metal transfer, Mater. Des. 49 (2013) 602–612.

[8] S. Niu, S. Chen, H. Dong, D. Zhao, X. Zhang, X. Guo, G. Wang, Microstructure and properties of lap joint between aluminum alloy and galvanized steel by CMT, J. Mater. Eng. Perform. 25 (5) (2016) 1839–1847.

[9] Y. Shi, J. Li, G. Zhang, J. Huang, Y. Gu, Corrosion behavior of aluminum-steel weld-brazing joint, J. Mater. Eng. Perform. 25 (5) (2016) 1916–1923.

[10] G. Zhang, M. Chen, Y. Shi, J. Huang, F. Yang, Analysis and modeling of the growth of intermetallic compounds in aluminum-steel joints, RSC Adv. 7 (60) (2017) 37797–37805.

[11] S. Lan, X. Liu, J. Ni, Microstructural evolution during friction stir welding of dissimilar aluminum alloy to advanced high-strength steel, Int. J. Adv. Manuf. Technol. 82 (9–12) (2016) 2183–2193.

[12] G. Sorger, H. Wang, P. Vilaça, T.G. Santos, FSW of aluminum AA5754 to steel DX54 with innovative overlap joint, Welding in the World 61 (2) (2017) 257–268.

[13] K.-K. Wang, L. Chang, D. Gan, H.-P. Wang, Heteroepitaxial growth of Fe_2Al_5 inhibition layer in hot-dip galvanizing of an interstitial-free steel, Thin Solid Films 518 (8) (2010) 1935–1942.

[14] A. Bouayad, C. Gerometta, A. Belkebir, A. Ambari, Kinetic interactions between solid iron and molten aluminium, Mater. Sci. Eng.: A 363 (1) (2003) 53–61.

[15] D. Naoi, M. Kajihara, Growth behavior of Fe_2Al_5 during reactive diffusion between Fe and Al at solid-state temperatures, Mater. Sci. Eng.: A 459 (1) (2007) 375–382.

[16] Y. Chen, A. Gholinia, P. Prangnell, Interface structure and bonding in abrasion circle friction stir spot welding: a novel approach for rapid welding aluminium alloy to steel automotive sheet, Mater. Chem. Phys. 134 (1) (2012) 459–463.

[17] W.-J. Cheng, C.-J. Wang, Study of microstructure and phase evolution of hot-dipped aluminide mild steel during high-temperature diffusion using electron backscatter diffraction, Appl. Surf. Sci. 257 (10) (2011) 4663–4668.

[18] L. Agudo, D. Eyidi, C.H. Schmaranzer, E. Arenholz, N. Jank, J. Bruckner, A. R. Pyzalla, Intermetallic Fe_xAl_y-phases in a Steel/Al-alloy fusion weld, J. Mater. Sci. 42 (12) (2007) 4205–4214.

[19] L. Jelver, P.M. Larsen, D. Stradi, K. Stokbro, K.W. Jacobsen, Determination of low-strain interfaces via geometric matching, Phys. Rev. B 96 (8) (2017), 085306.

[20] K. Mathew, A.K. Singh, J.J. Gabriel, K. Choudhary, S.B. Sinnott, A.V. Davydov, F. Tavazza, R.G. Hennig, Mpinterfaces: A materials project based python tool for high-throughput computational screening of interfacial systems, Comput. Mater. Sci. 122 (2016) 183–190.

[21] D. Stradi, L. Jelver, S. Smidstrup, K. Stokbro, Method for determining optimal supercell representation of interfaces, J. Phys.: Condens. Matter 29 (18) (2017), 185901.

[22] A. Zur, T. McGill, Lattice match: An application to heteroepitaxy, J. Appl. Phys. 55 (2) (1984) 378–386.

[23] N.T. Taylor, F.H. Davies, I.E.M. Rudkin, C.J. Price, T.H. Chan, S.P. Hepplestone, Artemis: Ab initio restructuring tool enabling the modelling of interface structures, Comput. Phys. Commun. 257 (2020), 107515.

[24] F. Therrien, P. Graf, V. Stevanović, Matching crystal structures atom-to-atom, J. Chem. Phys. 152 (7) (2020), 074106.

[25] W. Bollmann, Crystal defects and crystalline interfaces, Springer Science & Business Media, 2012.

[26] W. Bollmann, O-lattice calculation of an FCC–BCC interface, Physica Status Solidi (a) 21 (2) (1974) 543–550.

[27] M.-X. Zhang, P.M. Kelly, M.A. Easton, J.A. Taylor, Crystallographic study of grain refinement in aluminum alloys using the edge-to-edge matching model, Acta Mater. 53 (5) (2005) 1427–1438.

[28] Y. Ikuhara, P. Pirouz, Orientation relationship in large mismatched bicrystals and coincidence of reciprocal lattice points (CRLP), in: Materials Science Forum, Vol. 207, Trans Tech Publications, 1996, pp. 121–124.

[29] M.Z. Khalid, J. Friis, P.H. Ninive, K. Marthinsen, A. Strandlie, Ab-initio study of atomic structure and mechanical behaviour of Al/Fe intermetallic interfaces, Comput. Mater. Sci. 174 (2020), 109481.

[30] M.Z. Khalid, J. Friis, P.H. Ninive, K. Marthinsen, A. Strandlie, First-principles study of tensile and shear strength of Fe-Al and α-AlFeSi intermetallic compound interfaces, Comput. Mater. Sci. 187 (2020), 110058.

[31] G. Kresse, J. Furthmüller, Vienna ab-initio simulation package (VASP), Vienna: Vienna University.

[32] J.P. Perdew, K. Burke, M. Ernzerhof, Generalized gradient approximation made simple, Phys. Rev. Lett. 77 (18) (1996) 3865.

[33] P.E. Blöchl, Projector augmented-wave method, Phys. Rev. B 50 (24) (1994) 17953.

[34] H.J. Monkhorst, J.D. Pack, Special points for brillouin-zone integrations, Phys. Rev. B 13 (12) (1976) 5188.

[35] U. Burkhardt, Y. Grin, M. Ellner, K. Peters, Structure refinement of the iron–aluminium phase with the approximate composition Fe_2Al_5, Acta Crystallographica Section B 50 (3) (1994) 313–316.

[36] Fe_2Al_5 (FeAl2.8) crystal structure: Datasheet from "pauling file multinaries edition – 2012" in springermaterials (https://materials.springer.com/isp/crystallographic/docs/sd_1201135), copyright 2016 Springer-Verlag, Berlin Heidelberg & Material Phases Data System (MPDS), Switzerland & National Institute for Materials Science (NIMS), Japan. https://materials.springer.com/isp/crystallographic/docs/sd_1201135.

[37] M.Z. Khalid, J. Friis, P.H. Ninive, K. Marthinsen, A. Strandlie, DFT calculations based insight into bonding character and strength of Fe_2Al_5 and Fe_4Al_{13} intermetallics at Al-Fe joints, Procedia Manuf. 15C (2018) 1407–1415.

[38] Y. Liu, X. Chong, Y. Jiang, R. Zhou, J. Feng, Mechanical properties and electronic structures of Fe-Al intermetallic, Physica B 506 (2017) 1–11.

[39] C.-H. Zhang, S. Huang, J. Shen, N.-X. Chen, Structural and mechanical properties of Fe-Al compounds: An atomistic study by EAM simulation, Intermetallics 52 (2014) 86–91.

[40] H. Okamoto, T. Massalski, et al., Binary alloy phase diagrams, ASM International, Materials Park, OH, USA.

[41] P. Lazar, R. Podloucky, Cleavage fracture of a crystal: Density functional theory calculations based on a model which includes structural relaxations, Phys. Rev. B 78 (10) (2008), 104114.

[42] R. Janisch, N. Ahmed, A. Hartmaier, Ab initio tensile tests of Al bulk crystals and grain boundaries: Universality of mechanical behavior, Phys. Rev. B 81 (18) (2010), 184108.

[43] M. Yamaguchi, First-principles study on the grain boundary embrittlement of metals by solute segregation: Part i. iron (Fe)-solute (B, C, P, and S) systems, Metallurgical and Materials Transactions A 42 (2) (2011) 319–329.

[44] J.H. Rose, J.R. Smith, J. Ferrante, Universal features of bonding in metals, Phys. Rev. B 28 (4) (1983) 1835.

[45] E.A. Jarvis, R.L. Hayes, E.A. Carter, Effects of oxidation on the nanoscale mechanisms of crack formation in aluminum, ChemPhysChem 2 (1) (2001) 55–59.

[46] I. J. Jensen, J. Friis, C. D. Marioara, I. G. Ringdalen, The role of grain boundary precipitates during intergranular fracture in 6XXX series Aluminium alloys, In preparation.

[47] D. Zhao, O.M. Løvvik, K. Marthinsen, Y. Li, Segregation of Mg, Cu and their effects on the strength of Al σ5 (210)[001] symmetrical tilt grain boundary, Acta Mater. 145 (2018) 235–246.

[48] R. Yang, S. Tanaka, M. Kohyama*, First-principles study on the tensile strength and fracture of the Al-terminated stoichiometric α-Al_2O_3 (0001)/Cu (111) interface, Philosophical Magazine 85 (25) (2005) 2961–2976.

[49] M. Černý, J. Pokluda, Ideal tensile strength of cubic crystals under superimposed transverse biaxial stresses from first principles, Phys. Rev. B 82 (17) (2010), 174106.

[50] S. Ogata, J. Li, N. Hirosaki, Y. Shibutani, S. Yip, Ideal shear strain of metals and ceramics, Phys. Rev. B 70 (10) (2004), 104104.

[51] M. Černý, P. Řehák, Y. Umeno, J. Pokluda, Stability and strength of covalent crystals under uniaxial and triaxial loading from first principles, J. Phys.: Condens. Matter 25 (3) (2012), 035401.

[52] P. Peyre, G. Sierra, F. Deschaux-Beaume, D. Stuart, G. Fras, Generation of aluminium-steel joints with laser-induced reactive wetting, Mater. Sci. Eng.: A 444 (1–2) (2007) 327–338.

[53] Y.-J. Wang, C.-Y. Wang, Influence of the alloying element re on the ideal tensile and shear strength of γ-Ni_3Al, Scripta Mater. 61 (2) (2009) 197–200.

[54] J. Hirth, R. Pond, R. Hoagland, X.-Y. Liu, J. Wang, Interface defects, reference spaces and the Frank-Bilby equation, Prog. Mater Sci. 58 (5) (2013) 749–823.

[55] W. Qian, X.-S. Leng, T.-H. Yang, J.-C. Yan, Effects of Fe—Al intermetallic compounds on interfacial bonding of clad materials, Trans. Nonferrous Metals Soc. China 24 (1) (2014) 279–284.

[56] M. Černý, J. Pokluda, On the effect of supercell size and strain localization in computational tensile tests, Modell. Simul. Mater. Sci. Eng. 28 (6) (2020), 065011.